Available online at www.sciencedirect.com
SCIENCE DIRECT®
ELSEVIER
Progress in Biophysics and Molecular Biology 90 (2006) 326–345
Progress in Biophysics & Molecular Biology
www.elsevier.com/locate/pbiomolbio

Review

Comparison of electrophysiological models for human ventricular cells and tissues

Kirsten H.W.J. Ten Tusscher[a,*], Olivier Bernus[b], Rok Hren[c], Alexander V. Panfilov[a]

[a]*Theoretical Biology, University of Utrecht, Padualaan 8, 3584 CH, Utrecht, The Netherlands*
[b]*Department of Pharmacology, SUNY Upstate Medical University, 750 East Adams St. (WHA), Syracuse, NY 13210, USA*
[c]*Department of Physics, Institute of Mathematics, Physics & Mechanics, University of Ljubljana, Jadranska 19, SI-1000 Ljubljana, Slovenia*

Available online 22 June 2005

Abstract

In this paper we briefly review currently published models for human ventricular cells and tissues. We discuss the Priebe–Beuckelmann (PB) model and the reduced version of this model constructed by Bernus et al. (redPB), the Ten Tusscher–Noble–Noble–Panfilov (TNNP) model and the Iyer–Mazhari–Winslow (IMW) model. We compare several characteristics of these models such as: sources of experimental data the models are based on, action potential morphology, action potential duration (APD) and conduction velocity (CV) restitution and computational efficiency. Finally, we discuss the application of a subset of these models—the redPB and the TNNP model—to study simulated spiral wave dynamics in 2D tissue sheets and in the human ventricles. We discuss the suitability of the different models for particular research questions and their limitations.

Keywords: Electrophysiology; Human ventricular cell; Arrhythmia; Re-entry; Mathematical model

*Corresponding author.
E-mail addresses: khwjtuss@hotmail.com (K.H.W.J. Ten Tusscher), bernuso@upstate.edu (O. Bernus), hren@fiz.uni-lj.si (R. Hren), A.V.Panfilov@bio.uu.nl (A.V. Panfilov).
URL: http://www-binf.bio.uu.nl/khwjtuss, http://www.fiz.uni-lj.si/bio/hren/, http://www-binf.bio.uu.nl/panfilov.

0079-6107/$ - see front matter © 2005 Elsevier Ltd. All rights reserved.
doi:10.1016/j.pbiomolbio.2005.05.015

Contents

1. Introduction

Sudden cardiac death is a major cause of death in the industrialized world. In most cases sudden cardiac death is caused by cardiac arrhythmias, mainly ventricular tachycardia (VT) degenerating into ventricular fibrillation (VF) or immediately occurring VF (Gettes et al., 1995). It is now widely accepted that most dangerous cardiac arrhythmias are associated with abnormal wave propagation caused by reentrant sources of excitation (Jalife, 2000). The mechanisms underlying the initiation and subsequent dynamics of these reentrant sources in the human heart are largely unknown, primarily due to the limited possibilities of invasively studying cardiac arrhythmias in humans. Consequently, a lot of research has been performed on animal hearts, ranging from the mouse, rat, guinea pig, rabbit, dog to the pig heart. However, the arrhythmias studied in animal hearts are not necessarily the same as those which occur in the human heart. For example, the frequency of VF in the human heart is about 5 Hz (Clayton et al., 1995a, b; Nanthakumar et al., 2004), whereas VF in the pig heart has a frequency of 10–14 Hz (Valderrabano et al., 2002; Rogers et al., 2003), despite the fact that the pig heart is of a size comparable to the human heart.

Another major limitation of any experimental study of ventricular arrhythmias is that patterns of excitation can be recorded with reasonable resolution only from the surface of the heart, whereas the underlying excitation patterns are 3D. Although some work has been done to overcome these limitations—either using transmural plunge needle electrodes (Newton et al., 2004) or transillumination in combination with optical mapping (Baxter et al., 2001)—the spatial resolution of current 3D measurement techniques is insufficient to identify the reentrant sources of arrhythmias and to study their dynamics. Computer modeling, especially detailed quantitative modeling of the human heart, can play an important role in overcoming these types of limitations.

The core of any cardiac arrhythmia modeling study is a model describing electrodynamical properties of the cardiac cell. Due to the limited availability of human cardiomyocytes for experimental research, most detailed electrophysiological models have been formulated for animal cardiomyocytes. For example, the Noble model (Noble et al., 1998) and the Luo–Rudy models (Luo and Rudy, 1991, 1994) were formulated for guinea pig ventricular cells, whereas the Winslow (Winslow et al., 1999) model was formulated for canine ventricular cells. However, animal cardiomyocytes differ from human ones in important aspects such as action potential shape and duration, range of normal heart rates, action potential restitution and relative importance of ionic currents in the action potential generation. As these factors may influence the mechanism of arrhythmia initiation and dynamics, models of human ventricular myocytes are much needed.

In recent years more and more data on human ionic currents have been gathered from human cardiomyocytes. In addition, a new technique has been developed, involving the cloning of human ion channels and heterologously expressing them in another cell type from which then voltage clamp measurements can be made. As a consequence, in recent years, several models for human ventricular cells have been formulated. In 1998 Priebe and Beuckelmann published the first model for human ventricular myocytes (Priebe and Beuckelmann, 1998) (PB model). Their model was largely based on the Luo–Rudy phase 2 model for guinea pig ventricular cells (Luo and Rudy, 1994) in which formulations for the major ionic currents were adjusted to the scarce data available for human ventricular cells at that time. In addition, for the computer power available at that time, the model was too complex for large-scale spatial simulations of reentrant arrhythmias.

This limitation was overcome in a reduced version of the PB model proposed by Bernus et al. (2002b) (redPB model), where the number of variables was reduced from 15 to 6 by reformulating some currents and fixating intracellular ionic concentrations. Early 2004, a new model for human ventricular myocytes by Ten Tusscher, Noble, Noble and Panfilov appeared (Ten Tusscher et al., 2004) (TNNP model). This model uses new formulations for all major ionic currents based on a now much wider basis of experimental data, largely from human ventricular cell experiments but also from ion channel expression experiments. The TNNP model was formulated for the purpose of performing large-scale spatial simulations. Therefore, it was constructed to form a compromise between a considerable level of physiological detail and computational efficiency. Later on in 2004 another model for human ventricular myocytes by Iyer et al. (2004) (IMW model) was published. As compared to the TNNP model, the IMW model is more strongly based on expression data on human cardiac ion channels than on data on human ventricular cells. In addition, formulations for most major ionic current are of the Markov chain rather than Hodgkin–Huxley type, causing the model to consist of a larger number of variables: 67 in the IMW model compared to 16 in the TNNP model.

In this paper we will perform a comparison of the above-mentioned models for human ventricular cells and their application in studies of cardiac arrhythmias. We will compare the sources of experimental data used to formulate the models, the differences in action potential morphology and duration, differences in action potential and conduction velocity restitution, differences in response to I_{Ks} and I_{Kr} current blocks and the differences in computational efficiency of the different models. We will also compare published and provide new results on the application of a subset of these models in studies of reentrant ventricular arrhythmias in 2D tissue

sheets and 3D anatomically accurate models of the human ventricles. We end with a discussion of the suitability of the different models to study different research questions and their limitations.

2. Methods

2.1. Mathematical modeling

The excitation process of a cardiac cell is governed by the flux of charged ions (predominantly Na^+, K^+, Ca^{2+} and Cl^-) through protein channels in the cell membrane. This ion flux leads to a change in transmembrane potential. This process can be mathematically described using the following differential equation (Keener and Sneyd, 1998):

$$\frac{dV}{dt} = -\frac{I_{ion} + I}{C_m}, \tag{1}$$

where C_m is the membrane capacitance, V is the transmembrane potential, I is the externally applied transmembrane current and I_{ion} is the sum of all transmembrane ionic currents. Integration of Eq. (1) gives us the time course of excitation of a single cardiac cell.

In cardiac tissue, the excitation wave spreads through the tissue because the cardiac cells are electrically coupled via gap junctions. To describe the propagation of the excitation wave, Eq. (1) needs to be extended to incorporate the axial current flow between cardiac cells. This incorporation of axial currents is usually approximated as follows (Keener and Sneyd, 1998):

$$\frac{\partial V}{\partial t} = -\frac{I_{ion} + I}{C_m} + \nabla D \nabla V, \tag{2}$$

where D is a tensor describing the conductivity of the tissue and ∇ is the 1D, 2D or 3D gradient operator. Integration of Eq. (2) gives us (i) the time course of excitation and (ii) propagation of excitation in multicellular cardiac tissue.

To simulate cell and tissue behavior following the different models, different sets of transmembrane current equations (equations together making up I_{ion}) as described in the PB, redPB, TNNP and IMW model were used. For a detailed description of these equations we refer to the original papers in which these equations were first introduced (Priebe and Beuckelmann, 1998; Bernus et al., 2002b; Ten Tusscher et al., 2004; Iyer et al., 2004). In addition, we will include a particular modified version of the redPB model in part of our comparisons. This model was used for simulations of reentrant arrhythmias in the complete human ventricles (Bernus et al., 2004). This modified version of the redPB model differs from the original redPB model in two aspects. First of all, it is a so-called γ-model, in which a factor γ is used to rescale the fast sodium current dynamics, thus reducing the stiffness of the model and hence increasing the computational efficiency (described in Bernus et al., 2002a). Second, the parameter settings have been changed relative to the original redPB model in order to obtain a shorter action potential duration (APD) (270 ms at 1 Hz) (described in Bernus et al., 2004). We will refer to this model as the γ-redPB model.

In 1D simulations $D = D_L$, with the D_L value chosen such that we obtained a (longitudinal) conduction velocity of approximately 70 cm s^{-1} as was experimentally reported by Jongsma and

Wilders (2000) for human ventricular tissue. This requires $D_L = 1.389\,cm^2\,s^{-1}$ for the PB and redPB model, and $D_L = 1.543\,cm^2\,s^{-1}$ for the TNNP model. In 2D simulations, isotropic tissue sheets were modeled by taking $D_{ij} = D_L\delta_{ij}$, where δ_{ij} is the unitary tensor, and D_L has the same value as in 1D. In simulations involving the complete human ventricles, muscle fiber direction anisotropy was taken into account. Assuming that transverse conductivity is the same in all directions orthogonal to the direction of the muscle fiber axis, we described the ventricular conductivity tensor using the following equation:

$$D_{ij} = D_T * \delta_{i,j} + (D_L - D_T)\alpha_i\alpha_j, \tag{3}$$

where α is a unit vector in the muscle fiber direction, and D_L is the conductivity in the longitudinal and D_T the conductivity in the transversal fiber direction, respectively. We use a ratio of 2:1 or 3:1 for the anisotropy of conduction velocities and hence a ratio of 4:1 or 9:1 for D_L: D_T. D_L has the same value as in 1D and 2D.

Data describing the human ventricular geometry and muscle fiber direction field were obtained by Hren (1996) from a structurally normal human heart. The conductivity tensor at each position was derived from the local muscle fiber direction field using Eq. (3). The geometry and conductivity data were validated by Hren (1996) by comparing the simulated with the experimentally observed normal excitation sequence in the human heart (Durrer et al., 1970).

2.2. Numerical approach

For single cell computations, Euler forward integration was used to update voltage and concentration states, and the channel states of the Markov chain channels of the IMW model. To integrate the Hodgkin–Huxley-type equations of the various gating variables in the PB, redPB, γ-redPB and TNNP model the Rush and Larsen integration scheme was used (Rush and Larsen, 1978). For the IMW model a time step of $\Delta t = 0.00002$ ms was required for stable and precise integration, for the other models a time step of $\Delta t = 0.02$ ms could be used. For 1D and 2D simulations Eq. (2) was integrated using a simple Euler forward scheme with a time step of $\Delta t = 0.02$ ms and a space step of $\Delta x = 0.2$ mm for the PB, redPB and TNNP models, and a time step of $\Delta t = 0.06$ ms and a space step of $\Delta x = 0.5$ mm for the γ-redPB model. Because of the different space steps, field sizes of 1200×1200 were used for the redPB and TNNP models in 2D, and field sizes of 500×500 were used for the γ-redPB model. For the whole ventricle simulations, to speed up computations, Eq. (2) was integrated using operator splitting for the reaction diffusion equations combined with time-adaptive Euler forward integration of the reaction ordinary differential equation (described in Qu and Garfinkel, 1999; Ten Tusscher and Panfilov, 2003). The diffusion partial differential equation (PDE) was integrated using a single constant time step. Integration of this PDE requires the evaluation of the following Laplacian in each point of the ventricular geometry:

$$\Delta(i,j,k) = \frac{\partial}{\partial x_i} D_{ij} \frac{\partial}{\partial x_j} V_m. \tag{4}$$

This Laplacian can be discretized to the following equation:

$$L(i,j,k) = \sum_{l=0}^{18} w_l V_m(l), \tag{5}$$

where l is an index running over the 18 neighbors of the point (i,j,k) and the point itself and w_l is the weight with which a neighbor grid point contributes to the Laplacian. The weights w_l are computed based on the conductivity tensor and the boundary situation in the point (i,j,k). No flux boundary conditions ensuring a zero axial-current flow from heart points to non-heart points are accomplished by giving a neighbor l that lies outside the heart geometry a weight $w_l = 0$. Given that in a non-contracting heart model conductivity and boundaries stay constant, these weights can be precomputed, stored, and used in simulations as an efficient means to evaluate the Laplacian and automatically handle boundary conditions. For whole ventricle simulations using the γ-redPB model, a space step of $\Delta x = 0.5$ mm a minimum time step of $\Delta t_{min} = 0.01$ ms and a maximum time step of $\Delta t_{max} = 0.04$ ms is used in a $217 \times 217 \times 217$ voxel grid encompassing the heart geometry, for simulations using the TNNP model a space step of $\Delta x = 0.25$ mm, a minimum time step of $\Delta t_{min} = 0.02$ ms and a maximum time step of $\Delta t_{max} = 0.1$ ms is used in a $434 \times 434 \times 434$ voxel grid.

APD is defined as action potential duration at 90% repolarization (APD_{90}). The so-called S1–S2 protocol was used to determine APD restitution (APDR) in single cells. The protocol consists of 10 S1 stimuli applied at a basic cycle length (BCL) of 1000 ms and a strength of two times the threshold value, followed by a S2 extra-stimulus delivered at some diastolic interval (DI) after the AP generated by the last S1 stimulus. The APDR curve is generated by decreasing DI and plotting APD generated by the S2 stimulus against DI. CV restitution (CVR) was determined by applying a so-called dynamic restitution protocol to a cable of 400 cells that was placed at one end. The protocol consists of a series of stimuli at a certain BCL until a steady-state CV is reached; after that, the cycle length is decreased. The CVR curve is obtained by plotting steady-state CV against steady-state DIs.

2D spiral waves and 3D scroll waves were initiated using a S1–S2 stimulus protocol, with the S2 stimulus applied in the refractory tail of the S1 wave. Stimulus current strengths were at twice the diastolic threshold. Electrograms were obtained by assuming an infinite volume conductor and calculating the dipole source density of the membrane potential V_m in all node points of the medium using the following equation (Plonsey and Barr, 1989):

$$\mathrm{ECG} = \int_V \frac{D\nabla V_m \cdot \vec{r}}{r^3}\,\mathrm{d}V, \tag{6}$$

where V is the volume (for the ventricles) or area (for the 2D tissue sheets) over which is integrated, and $\vec{r}$ is the vector from the recording electrode to a point in the tissue. For the 2D tissue we placed the recording electrode 10 cm above the middle of the sheet, for the ventricles it was placed 10 cm from the center of the ventricles in the transverse plane.

In the tissue sheet simulations, spiral wave tips were traced using an algorithm proposed by Fenton and Karma (1998), by detecting spiral tip points as the intersection point of an isopotential line (in our case -35 mV) and the $\mathrm{d}V/\mathrm{d}t = 0$ line.

The single cell, cable, tissue sheet simulations and the whole ventricle simulations using the γ-redPB model were coded in C++ and run on a single processor of a Dell 650 Precision Workstation (dual Intel xeon 2.66 GHz). The 3D ventricular simulations using the TNNP model were coded in C++ and MPI and were run on eight processors of a Beowulf cluster consisting of four Dell 650 Precision Workstations (dual Intel xeon 2.66 GHz). In 3D, ventricular geometry and wave patterns were visualized using the marching cube algorithm for isosurface detection in voxel data and OpenGL for isosurface drawing.

3. Results

3.1. Experimental basis

Table 1 shows the sources of experimental data for the PB, TNNP and IMW models. Note, that the redPB model and γ-redPB model are derived from the PB model and hence are based on the same data sets. The main sources of experimental data used to construct these human ventricular cell models are: voltage clamp experiments on animal cardiomyocytes (A), voltage clamp experiments on human ventricular myocytes (H), and voltage clamp experiments on cells in which cloned human cardiac ion channels are heterologously expressed (C). If multiple data sets of the same type were used for a single current, this is designated by the multiple use of that particular character symbol.

We see that all three models largely make use of human-based experimental data. However, there are some important differences. One specific difference is in the data used for the fast sodium current formulation. The PB model uses an I_{Na} current formulation based mainly on chicken embryo cardiomyocyte data. The TNNP model uses both human myocyte and heterologous expression data for its I_{Na} formulation. The IMW model I_{Na} formulation is based on heterologously expressed human I_{Na} channel data. In general, most PB model current formulations are based on a single H data set, the TNNP model current formulations are based on multiple H data sets that are sometimes combined with C data sets, and most IMW model current formulations are based on single or multiple C data sets. H and C-type data sets each have their own advantages and disadvantages. H data sets require cell isolation and blocking of other currents by prepulses or chemicals which all may affect the current under study. For C data sets these procedures are not needed, but instead ionic currents are studied outside their natural cellular environment. Ideally, both types of data should be used to construct current formulations.

Table 1
Experimental data used as a basis for the PB, TNNP and IMW model

Current	PB model	TNNP model	IMW model
I_{Na}	A,A	H,H,C,C,C,C	C,C
I_{to}	H	H,H	C,C
I_{CaL}	H	H,H,H,H,H,H,H	H,H,A
I_{Kr}	H	H,H,C,C,C	C
I_{Ks}	H	H,H,H	C,C,C
I_{K1}	H	H,H	C

3.2. Model complexity and computational efficiency

An important difference between the PB, redPB, TNNP and the IMW model is their complexity and suitability for performing large-scale spatial simulations. The PB and TNNP model are of a similar complexity, they use Hodgkin–Huxley-type equations for the ionic currents and they model intracellular sodium, potassium and calcium dynamics. The PB model consists of 15 and the TNNP model of 16 variables. The redPB model is much simpler than these models. It was derived from the PB model by reducing the number of current gate variables, reformulating several ionic currents and fixating intracellular ion concentrations, thus reducing the number of variables from 15 to 6. The IMW model uses Markov chain models rather than Hodgkin–Huxley-type equations to describe the dynamics of the major ionic currents. While this allows one to fit single channel experimental data and to incorporate knowledge on ion channel structure (Iyer et al., 2004), this comes at the cost of a much higher number of variables, which is 67 in the case of the IMW model.

Apart from the number of variables, the computational efficiency of a model is also determined by the stiffness of its equations. The stiffness will determine how small integration time steps need to be in order to obtain a stable and precise enough solution of the model differential equations. We performed a comparison of the computational efficiency of the models under standard conditions, i.e. using simple Euler forward integration, which is the most widely used integration method for large-scale spatial simulations in electrophysiology. We found that the PB, redPB and TNNP model allowed for a much larger (0.02 ms) time step of integration than the IMW model (0.00002 ms). Together, the differences in variable numbers and integration time step sizes cause simulations with the PB and TNNP model to be approximately equally fast, cause the redPB model to be 2.2 times faster than the PB model, and cause the IMW model to be about 900 times slower than the PB model.

It should be noted that the numerical efficiency of all these models can be increased using a number of different possible numerical approaches. One example is the use of an adaptive time step for integration, adjusting time step size to changing stiffness of the equations for different variable values. Another example is the use of a so-called γ-version of the model, such as applied in Bernus et al. (2004) to the redPB model, in which fast sodium current dynamics is rescaled hence reducing the stiffness of the equations. These approaches will be particularly beneficial for stiff systems such as the IMW model. Therefore, the differences in computational efficiency of the different models may change if more sophisticated methods of integration are used.

3.3. Action potential characteristics

In Table 2 we compare important action potential characteristics at 1 Hz steady-state pacing for the epicardial cell type of the PB, redPB, γ-redPB, TNNP and IMW models. Properties studied are (minimum) membrane voltage during the diastolic interval (V_{dia}), maximum membrane voltage reached during the AP upstroke (V_{max}), minimum membrane voltage reached during the AP notch (V_{notch}), maximum membrane voltage reached during the AP plateau or dome phase ($V_{plateau}$), action potential amplitude (APA $= V_{max} - V_{dia}$) (all in mV) and APD (in ms). We also show the AP morphologies generated by the different models in Fig. 1a.

Table 2
Action potential characteristics of the PB, redPB, γ-redPB, TNNP and IMW model together with the (range of) experimentally found values (for sources see text)

Model	V_{dia}	V_{max}	V_{notch}	$V_{plateau}$	APA	APD
PB	−90.4	49.3	2.1	17.7	139.7	360
redPB	−90.3	38.3	9.0	21.2	128.6	360
γ-redPB	−91.9	34.2	7.9	16.76	126.1	270
TNNP	−86.3	31.7	12.9	21.6	118	270
IMW	−90.7	35.0	19.8	31.9	126	320
exp	−86	ND	ND	ND	95–104	270–350

We can see that action potential properties of the original PB and redPB model are very similar, particularly V_{dia}, $V_{plateau}$ and APD. Small differences in V_{max} and V_{notch} are caused by the slightly changed properties of I_{Na} and I_{to} current dynamics in the redPB model. The γ-redPB model has a shorter APD (270 versus 360 ms) due to its different parameter settings. Other action potential properties are very similar to the redPB model.

The PB, redPB, γ-redPB and IMW model all have a value of V_{dia} close to −90 mV, whereas the TNNP model has a value of −86.3 mV. Experimentally recorded values by Drouin et al. (1998) and Pereon et al. (2000) are around −86 mV. V_{max} values in the different models range from 31.7 (TNNP) to 49.3 mV (PB) resulting in action potential amplitudes ranging from 118 mV (TNNP) to 139.7 mV (PB). Drouin et al. (1998) and Pereon et al. (2000) report action potential amplitudes of 104 and 95 mV, respectively. V_{notch} values vary from 2.1 (PB) to 19.8 mV (IMW), with the TNNP model having an intermediate value of 12.9. $V_{plateau}$ values are around 20 mV for all models except the IMW model where the maximum plateau level is 31.9 mV. Note that elevated action potential plateau levels are found in cardiomyocytes from failing hearts (see, for example, Priebe and Beuckelmann, 1998). Putting the values of V_{max}, V_{notch} and $V_{plateau}$ together, and looking at Fig. 1a we can see that the PB model has the strongest spike-notch-dome shape, the IMW model has the least strong spike-notch-dome shape, and in the TNNP model this shape is intermediate.

APD varies from 270 ms in the TNNP and γ-redPB model, to 320 ms in the IMW model, to a value of 360 ms in the PB and redPB model. Experimentally reported APDs for (epicardial) human ventricular myocytes vary from around 270 (Li et al., 1998), to 325 (Pereon et al., 2000; Morgan et al., 1992; Franz et al., 1988; Li et al., 1996) to approximately 350 ms (Drouin et al., 1995; Li et al., 1999). Results are hard to interpret since they have often been obtained from myocytes from diseased hearts, and heart failure is known to prolong APD. In addition, some results are for single cells with all three ventricular cell types mixed together (336 ms, Li et al., 1996; 355 ms, Li et al., 1999), other results are for single cells, where cells were first split out into epicardial, endocardial and M cells (270 ms for epicardial cells, Li et al., 1998), other results are for transmural tissue wedges where an epicardial region is distinguished (351, 324 ms, Drouin et al., 1995; Pereon et al., 2000), and yet other results are from endocardial intrapatient mappings (330 ms, Morgan et al., 1992; 320 ms, Franz et al., 1988).

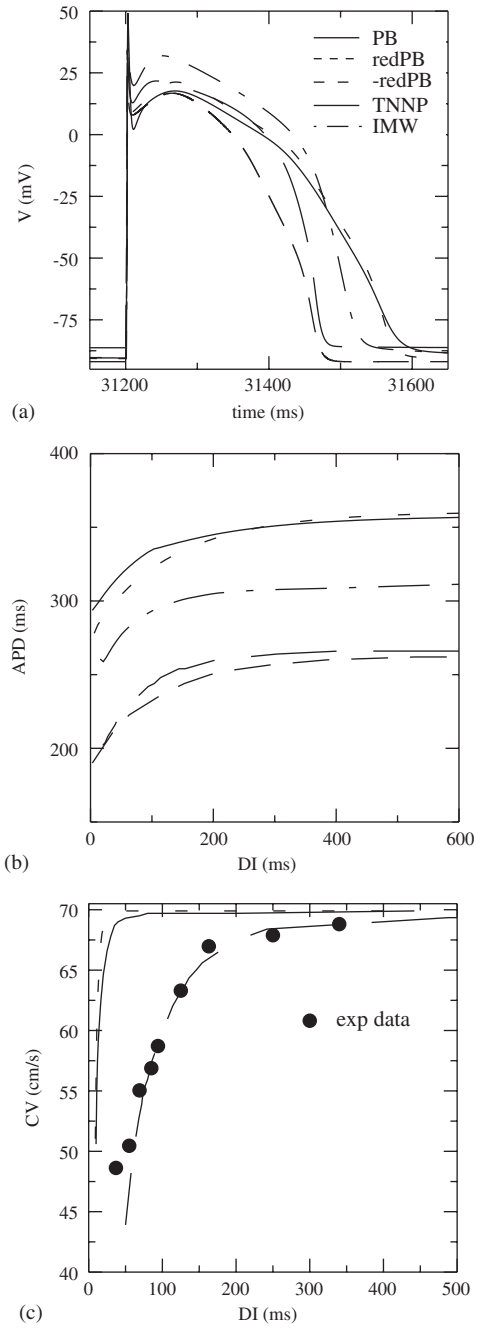

Fig. 1. (a) Action potential morphologies for the PB, redPB γ-redPB, TNNP and IMW models at 1 Hz steady-state pacing in a single cell. (b) Action potential duration restitution curves for the PB, redPB, γ-redPB, TNNP and IMW models obtained using a S1S2 protocol at a BCL of 1000 ms in a single cell. (c) Conduction velocity restitution curves for the PB, redPB and TNNP models obtained using a dynamic restitution protocol in a cable of 400 cells. Guinea pig experimental CV data from Girouard et al. (1996) are added for comparison. The experimental data are rescaled by a factor of 0.92 to get the same maximum CV level as in human ventricular tissue.

Table 3
Effect of I_{Ks} and I_{Kr} block on APD in the PB, TNNP and IMW model together with the (range of) experimentally found values (for sources see text)

Model	I_{Ks} block			I_{Kr} block		
	25%	50%	100%	25%	50%	100%
PB	15 ms	33 ms	93 ms	31 ms	74 ms	253 ms
	4.1%	9.2%	26.2%	8.8%	20.8%	70.9%
TNNP	12 ms	30 ms	102 ms	10 ms	20 ms	46 ms
	4.5%	11.3%	37.6%	3.7%	7.4%	17.0%
IMW	5 ms	11 ms	24 ms	7 ms	16 ms	35 ms
	1.6%	3.5%	7.7%	2.2%	5.1%	11.2%
exp	ND	ND	140 ms	ND	ND	47–88 ms
	ND	ND	40%	ND	ND	11–26%

3.4. Response to I_{Ks} and I_{Kr} block

In this review we do not intend to perform a detailed comparison of the effects of changing a large range of parameters of the different models on model behavior. However, we did perform a comparison of the effects of I_{Ks} and I_{Kr} current block on APD as these current are considered to be of great importance in determining differences between M cells and other cell types and determining ventricular transmural heterogeneity. Table 3 shows the effect of blocking either I_{Ks} or I_{Kr} current for 25%, 50% or 100% on APD. Note that we excluded the redPB and γ-redPB model from this comparison, as in these models the I_{Kr} and I_{Ks} currents have been merged into a single I_K current. Action potential prolongation is given both in ms and as percentage increase relative to normal 1 Hz steady-state APD.

We can see that the effects of blocking I_{Ks} and I_{Kr} current on APD are quite different for the different models. Blocking I_{Ks} current has most effect on APD in the TNNP model (37.6%) and least effect in the IMW model (7.7%). Bosch et al. (1998) performed the only experimental study on I_{Ks} block in human ventricular cells and reported an APD prolongation of approximately 40% (140 ms). The results from the TNNP model are in agreement with these data, while the PB model slightly and the IMW model strongly underestimate the importance of I_{Ks} on action potential repolarization. I_{Kr} current block has most effect on APD in the PB model (70.9%) and least effect in the IMW model (11.2%). Li et al. (1996) reported an APD prolongation of 26% (88 ms) upon full I_{Kr} block, whereas Iost et al. (1998) reported an APD prolongation of 11% (47 ms). The results from the TNNP and IMW model thus agree with the experimental data, whereas the effect of I_{Kr} block in the PB model is on the large side.

3.5. APD restitution

In Fig. 1b we show action potential restitution curves for the PB, redPB, γ-redPB, TNNP and IMW models. Curves were obtained by applying the S1S2 restitution protocol at a BCL of 1000 ms. The curves differ in the maximum APD level, as already discussed in Section 3.3, with the PB and redPB model having the longest, the TNNP model and γ-redPB model the shortest

and the IMW model having an intermediate APD. We can also see that all restitution curves have a similar shape with approximately similar slopes, with maximum slopes varying from a smallest value of 0.59 for the PB model to a largest value of 0.73 for the TNNP model.

Experimental APD restitution curves vary over a similar range as the model curves,which is demonstrated by the fact that both the PB and redPB restitution curves and the TNNP restitution curve are close fits to particular experimentally obtained restitution curves (see Fig. 10 in Priebe and Beuckelmann (1998), Fig. 4a in Bernus et al. (2002b), and Fig. 8 in Ten Tusscher et al. (2004)).

3.6. CV restitution

In Fig. 1c we show conduction velocity (CV) restitution curves obtained for the PB, redPB and TNNP models. We were not able to obtain a CV restitution curve for the IMW model due to its large computational requirements. We can see that the CV restitution curve in the redPB model has a slightly steeper slope and starts declining at slightly smaller diastolic intervals than the CV restitution curve of the original PB model due to its reformulated I_{Na} gating dynamics. Both curves show a CV that is constant over a large range of DIs and than suddenly plummets for short DIs. The γ-redPB model has a CV restitution curve that is very similar to that of the original redPB model (not shown here, see Fig. 4b in Bernus et al., 2002a). In contrast, the CV restitution curve of the TNNP model starts decreasing for much larger DIs and hence decreases more gradually and over a broader range of DIs. This is due to the much slower recovery dynamics of the I_{Na} j gate in the TNNP model. It has been shown in both dog and guinea pig ventricular tissue that CV restitution indeed decreases gradually (Cao et al., 1999; Girouard et al., 1996). In the graph, the guinea pig experimental data (Girouard et al., 1996) have been added, demonstrating a good agreement between the data and the TNNP CV restitution curve.

3.7. 2D tissue sheets

So far simulations of reentrant excitation patterns (spiral waves) in 2D tissue sheets were performed only in the redPB and the TNNP model (Bernus et al., 2002b; Ten Tusscher et al., 2004). In both cases, application of a S1S2 protocol led to formation of stable stationary rotating spiral waves with an average period of 304 ms in the redPB model and of 265 ms in the TNNP model. Here we also present new data on 2D spiral wave rotation in the γ-redPB model, where the period of spiral wave rotation is around 200 ms. The differences in spiral wave rotation period between these different models reflect both differences in APD and tissue recovery properties. In all three models, the spiral wave tip patterns showed a substantial degree of meandering.

Fig. 2 shows core patterns traced by the spiral tips of the redPB, TNNP and γ-redPB model. We can see that the redPB model (Fig. 2a) has a linear core pattern with a characteristic size of approximately 5 cm. The tip of the spiral wave follows a semi-straight line of block whose orientation slowly rotates in the course of time. In the TNNP model (Fig. 2b), the tip of the spiral wave followed a so-called Z-type core pattern consisting of semi-straight lines of block followed by semi-circular rotations. The size of the core pattern was approximately 3 cm. The TNNP core pattern also performs a rotation of its orientation over the course of time (Fig. 2c) The size of the core pattern ($\sim$2.5 cm) in the γ-redPB model is close to that in the TNNP model. The shape of the

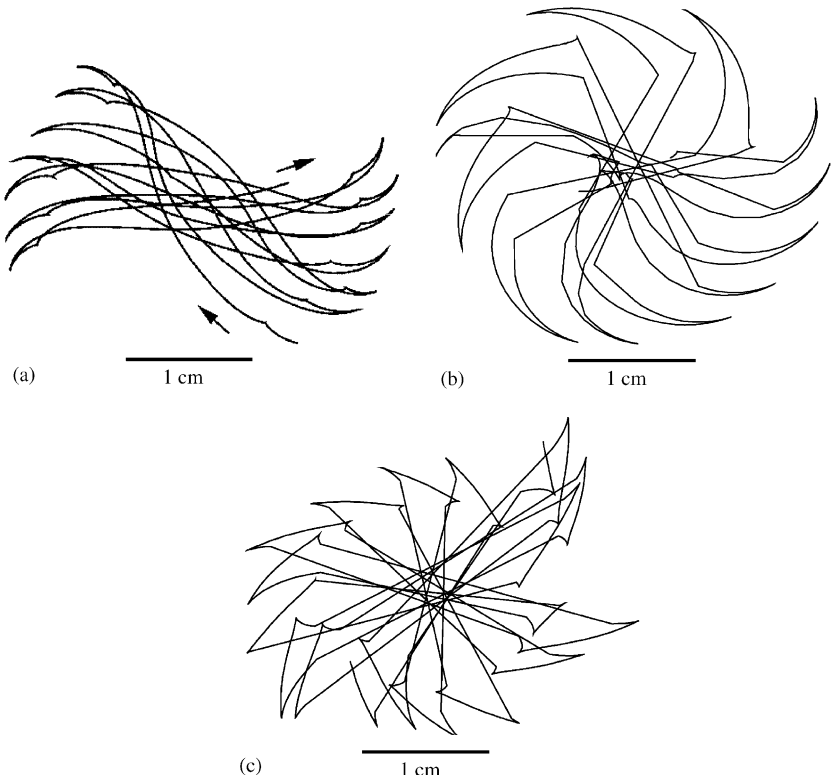

Fig. 2. Spiral tip core patterns for the (a) redPB (b) TNNP and (c) γ-redPB model. Figures (a) and (b) are reproduced with permission from Bernus et al. (2002b) and Ten Tusscher et al. (2004), respectively.

core pattern is somewhere in between the linear core pattern of the redPB model and the Z-type core pattern of the TNNP model.

The relation of the core pattern to the properties of cardiac cells is a complex question which is not yet completely understood. However, in Efimov et al. (1995) it was shown that a reduction of the fast sodium current reduces the size of the core of a spiral wave and results in the transition from a linear to a Z and finally a circular core meandering pattern. The TNNP model has a longer reactivation time for sodium current than the redPB model, which effectively reduces the sodium current during spiral wave rotation. Similarly, the γ-redPB model has a slower activation rate of the sodium current than the redPB model, also resulting in an effective reduction. Therefore, the differences in core pattern sizes and shapes between the models is likely to be at least partly due to these differences in the fast sodium current dynamics. In addition, the shorter APD of the TNNP and γ-redPB model compared to that of the redPB model may have contributed to the differences in core size. Spiral wave meander pattern is an important property which is believed to determine the type of cardiac arrhythmia (Abildskov and Lux, 1991; Gray et al., 1995; Garfinkel and Qu, 1999). Unfortunately, there are no data so far on meandering of spiral waves in experimental preparations of human cardiac tissue.

3.8. Whole ventricles

Simulations of scroll waves in anatomical models of human ventricles have so far been performed only using the γ-redPB model (Bernus et al., 2004) and the TNNP model (new results in this article). Scroll waves were initiated using a S1S2 protocol. To create a scroll wave in the right ventricular free wall, first a S1-stimulus was applied in the posterior part of the right ventricle. Then a S2-stimulus was applied to the refractory tail of the S1-wave, generating a vast area of unidirectional block at a predefined site in the right lateral ventricular wall, parallel to the S1 wave back and with the base of the ventricles as a boundary. The S2-wave "curled" around this area of block forming a scroll wave in the right lateral ventricular wall. Fig. 3a shows a spiral

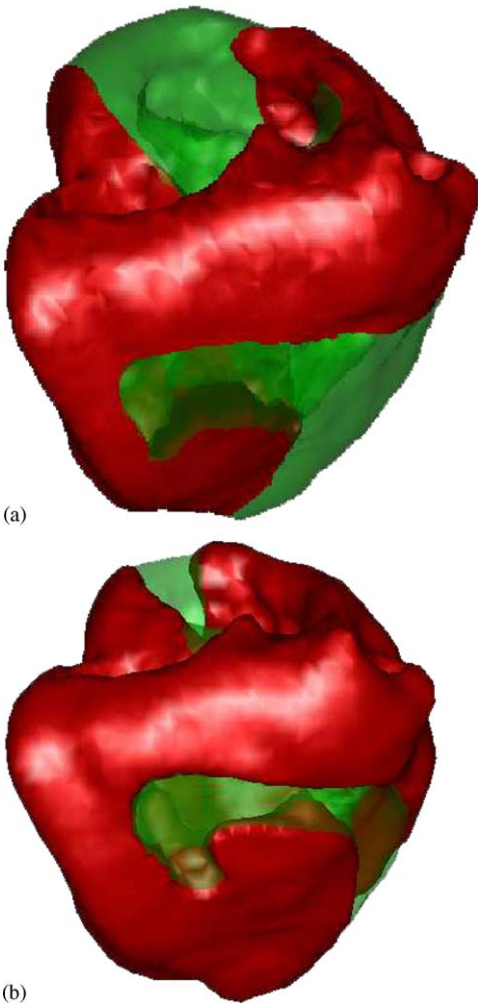

Fig. 3. Snapshots of spiral wave activity in the right ventricle (a) in the γ-redPB model (b) and the TNNP model. In the γ-redPB model an anisotropy ratio of 1:9 and a grid of $217 \times 217 \times 217$ with a space step of $\Delta x = 0.5$ mm was used, in the TNNP model an anisotropy ratio of 1:4 and a grid of $434 \times 434 \times 434$ with a space step of $\Delta x = 0.25$ mm was used.

wave located in the free wall of the right ventricle close to apex of the heart in the γ-redPB model. Fig. 3b shows similar results for the TNNP model. The ECG of the right ventricular scroll wave in the γ-redPB model is shown in Fig. 4a. It has a dominant frequency of 4.5 Hz, with small variations in amplitude and shape. Fig. 4c shows the ECG of the right ventricular scroll wave simulated with the TNNP model, which has a dominant frequency of 3.7 Hz, with regular amplitude and shape. Clinically recorded ECGs from patients with monomorphic ventricular tachycardia have a regular pattern and dominant activation frequency of 3.8 Hz (Clayton et al., 1995b). The results of the TNNP model are in close agreement with these data.

A vortex in the left ventricular wall can be created by applying an S1-stimulus at the posterior side of the ventricles and an S2-stimulus in the left lateral ventricle. In the γ-redPB model, this led to a strongly drifting scroll wave that disappeared after a few rotations. Fig. 4b shows the ECG corresponding to these excitation dynamics, where a return to the quiescent state after a few rotations can be seen. In contrast, in the TNNP model, initiation of a scroll wave in the left ventricle led to sustained scroll wave dynamics. However, when comparing the ECG corresponding to the scroll wave activity in the left ventricle (Fig. 4d) to the ECG of the scroll wave in the right ventricle (Fig. 4c), it can be seen that the scroll wave dynamics in the left ventricle is less regular than in the right ventricle. The ECG corresponding to the left ventricular scroll wave simulated in the TNNP model has a frequency of 3.6 Hz and resembles clinically recorded ECGs of polymorphic rather than monomorphic ventricular tachycardia (Clayton et al., 1995b).

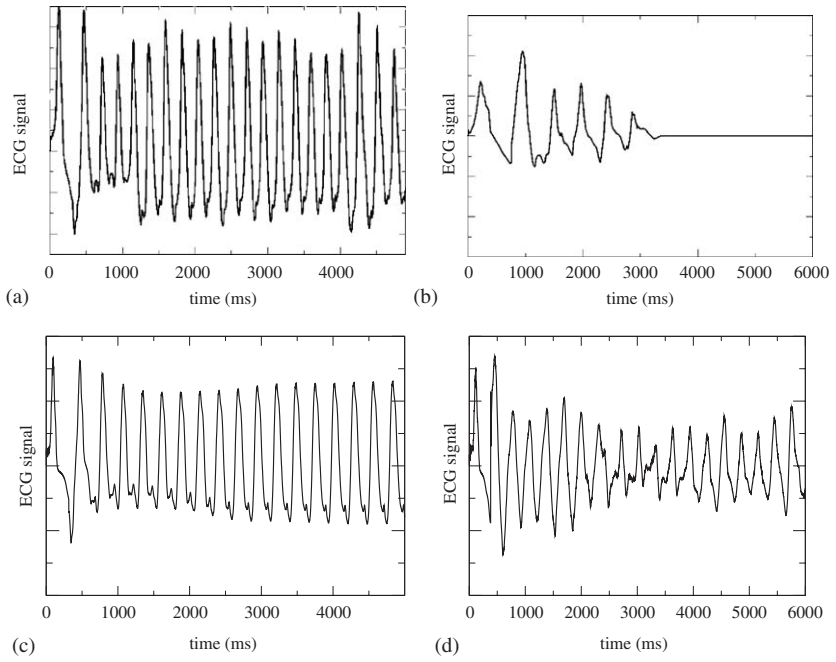

Fig. 4. ECGs of spiral wave activity. Top row (a,b) ECGs of spiral waves in the γ-redPB model, bottom row (c,d) ECGs of spiral waves in the TNNP model. Left column (a,c) ECGs of spiral wave activity in the right ventricle, right column (b,d) ECGs of spiral wave activity in the left ventricle. Figures (a) and (b) are reproduced with permission from Bernus et al. (2004).

A possible explanation of the fact that scroll waves in the left ventricle are less stable than in the right ventricle in both the γ-redPB and TNNP model may be the larger thickness of the left ventricular wall, which is known to increase scroll wave instability (Panfilov and Hogeweg, 1996; Panfilov and Keener, 1995). However, a larger number of simulations is required to accurately establish this.

4. Discussion

4.1. Pros and cons of the different models

In this paper we performed a brief comparison of the currently available models for human ventricular cells and tissues, the Priebe–Beuckelmann model and reduced versions of this model, the Ten Tusscher–Noble–Noble–Panfilov model and the Iyer–Mazhari–Winslow model. A logical and important question for anyone interested in performing simulations on human ventricular cells and tissues is which of these models to use. Each of the models has its advantages and disadvantages, the model's applicability will thus depend on the problem to be solved.

Clearly, the γ-redPB model is computationally the most efficient since the number of variables has been significantly reduced (to 6) and model stiffness has been reduced through the γ rescaling factor. As a consequence, this model is fastest when one wants to perform large-scale spatial simulations, e.g. to investigate reentrant arrhythmia dynamics in the human ventricles. However, the reduced stiffness of the model may affect particular properties of reentrant waves, for example, the shape of the spiral wave meander pattern (see Fig. 2c).

Slightly less computationally efficient is the redPB model, which has a model stiffness comparable to that of the other models but still has only six state variables. Since no 2D and 3D simulations have been performed with the complete PB model, we cannot say whether the reduction has changed properties such as spiral wave meander pattern. The low number of variables of the redPB model comes at the cost of absent intracellular ion dynamics and simplified current dynamics. As a consequence the model cannot be used to study, for example, the effect of sodium or calcium overload conditions. Still a bit less computationally efficient, but including detailed current descriptions and intracellular ion dynamics, are the PB and TNNP models. Because the TNNP model appeared 6 years later than the PB model it relies on a much broader basis of experimental data (Table 1). Therefore, we consider the TNNP model to be more realistic for human ventricular tissue than the PB model. Important differences between the models are, for example, the response of the model to I_{Ks} and I_{Kr} block (Table 3) and the CV restitution dynamics (Fig. 1c), which are in closer agreement to available experimental data for the TNNP model.

The IMW model appeared last and relies on an almost equally broad set of human-based experimental data as the TNNP model. However, the IMW model uses predominantly expression data on cloned human cardiac ion channels, whereas the TNNP model uses mainly data on human ventricular myocytes (Table 1). In how far this difference influences modeled current properties and model realism was outside the scope of this paper, but remains an important issue to be studied. In addition, the IMW model uses Markov chain models rather than Hodgkin–Huxley-type equations to describe the dynamics of the major ionic currents. The

resulting large number of variables (67) and small time step required for integration makes this model computationally extremely demanding for use in spatial simulations. However, the increased level of detail may make these types of models more suited for particular research in single cell settings, for example, to study the effects of a drug for which it is known which channel state or transition rate it affects.

4.2. Limitations of current models and experimental data

There are some important issues for further experimental and modeling research given the different behaviors of the different models and either the variability or scarcity of available experimental data.

One important issue is APD. APD and CV together determine the excitation wavelength, which will play an important role in determining, for example, the number of spiral waves that fit on the heart during ventricular fibrillation. APD is therefore very important for the spatial organization occurring during ventricular reentrant arrhythmias. However, both the models and the experimental data show a rather broad range of variation in APD values (270–360 ms). It would be important to establish whether this is natural interperson or intraperson variation or whether it depends on heart conditions (disease), cell isolation procedures, etc.

Another important point of unclarity is the quantitative importance of I_{Ks} and I_{Kr} currents for APD. The TNNP model seems to be most consistent with experimental results on I_{Ks} and I_{Kr} block, with the IMW model deviating significantly for I_{Ks} and the PB model deviating significantly for I_{Kr} block. However, there are only two human-based experimental data sets for I_{Kr} and only one dataset for I_{Ks} block. Data from dog ventricular myocytes suggest that I_{Ks} is less important than the human data suggest, and becomes more important (though still less than in the human data) when beta-adrenergic stimulation occurs Cheng and Kodama, 2004; Volders et al., 2003. I_{Ks} and I_{Kr} are important currents for defining the differential behavior of M cells, and for the occurrence of EADs, propagation block and Torsade de Pointes upon drug induced or congenital I_{Ks} and I_{Kr} reduction (LQT-1 and LQT-2). Therefore, we need to get a better and more quantitative idea about the size of I_{Kr} and I_{Ks} currents in human ventricular cells, and how this depends on position in the heart, disease conditions and adrenergic innervation.

A final important issue is intracellular calcium cycling. Calcium dynamics can be very important for arrhythmia initiation and its subsequent dynamics, given its involvement in EAD and DAD formation (Volders et al., 1997), alternans (Shimizu and Antzelevitch, 1999; Pruvot et al., 2004; Diaz et al., 2004; Shiferaw et al., 2003) and wave instability (Chudin et al., 1999; Omichi et al., 2004). In recent years, models of intracellular calcium handling have become increasingly complex, modeling individual L-type calcium channels, Ryanodine channels, calcium release subunits, and their local, stochastic interactions (Rice et al., 1999; Greenstein and Winslow, 2002). Because of their computational complexity, most models, like the ones discussed here, only incorporate a simplified model of intracellular calcium dynamics. In addition, despite ongoing experimental and modeling research important knowledge on the exact mechanisms as for example calcium release termination and recovery is still lacking. To model the role of calcium dynamics in arrhythmia initiation and progression, a compact (computationally efficient enough for spatial simulations) model of calcium dynamics that is able to accurately describe both normal stable and abnormal alternating or spontaneously active behavior is needed.

Acknowledgements

We are grateful to Dr. R. Wilders for valuable discussions on important aspects of this paper. We are also indebted to Dr.V. Iyer, Dr. R. Mazhari and Prof. L. Winslow for making their model source code available. This research was supported by the Netherlands Organization for Scientific Research (NWO) through Grant number 635.100.004 of the Research Council for Physical Sciences (EW).

References

Abildskov, J.A., Lux, R.L., 1991. The mechanism of simulated torsade de pointes in a computer model of propagated excitation. J. Cardiovasc. Electrophysiol. 2, 224–237.

Baxter, W.T., Mironov, S.F., Zaitsev, A.V., Jalife, J., Pertsov, A.M., 2001. Visualizing excitation waves inside cardiac muscle using transillumination. Biophys. J. 80, 516–530.

Bernus, O., Verschelde, H., Panfilov, A., 2002a. Modified ionic models of cardiac tissue for efficient large scale computations. Phys. Med. Biol. 47, 1947–1959.

Bernus, O., Wilders, R., Zemlin, C.W., Verschelde, H., Panfilov, A.V., 2002b. A computationally efficient electrophysiological model of human ventricular cells. Am. J. Physiol. Heart Circ. Physiol. 282, H2296–H2308.

Bernus, O., Verschelde, H., Panfilov, A.V., 2004. Reentry in an anatomical model of the human ventricles. Int. J. Bif. Chaos 13, 3693–3702.

Bosch, R.F., Gaspo, R., Busch, A.E., Lang, H.J., Li, G., Nattel, S., 1998. Effects of chromanol 293B, a selective blocker of the slow component of the delayed rectifier K^+ current, on repolarization in human and guinea pig ventricular myoctyes. Cardiovasc. Res. 38, 441–450.

Cao, J., Qu, Z., Kim, Y., Wu, T., Garfinkel, A., Weiss, J.N., Karagueuzian, H.S., Chen, P., 1999. Spatiotemporal heterogeneity in the induction of ventricular fibrillation by rapid pacing, importance of cardiac restitution properties. Circ. Res. 84, 1318–1331.

Cheng, J., Kodama, I., 2004. Two components of delayed rectifier K^+ current in heart: molecular basis functional diversity and contribution to repolarization. Acta Pharmacol. Sin. 25, 137–145.

Chudin, E., Goldhaber, J., Garfinkel, A., Weiss, J., Kogan, B., 1999. Intracellular Ca^{2+} dynamics and the stability of ventricular tachycardia. Biophys. J. 77, 2930–2941.

Clayton, R.H., Murray, A., Campbell, R.W., 1995a. Analysis of the body surface ECG measured in independent leads during ventricular fibrillation in humans. Pacing Clin. Electrophysiol. 18, 1876–1881.

Clayton, R.H., Murray, A., Campbell, R.W., 1995b. Objective features of the surface electrocardiogram during ventricular tachyarrhythmias. Eur. Heart J. 16, 1115–1119.

Diaz, M.E., O'Neill, S.C., Eisner, D.A., 2004. Sarcoplasmic reticulum calcium content fluctuation is the key to cardiac alternans. Circ. Res. 94, 650–656.

Drouin, E., Charpentier, F., Gauthier, C., Laurent, K., Le Marec, H., 1995. Electrophysiologic characteristics of cells spanning the left ventricular wall of human heart: evidence for the presence of M cells. J. Am. Coll. Cardiol. 26, 185–192.

Drouin, E., Lande, G., Charpentier, F., 1998. Amiodarone reduces transmural heterogeneity of repolarization in the human heart. J. Am. Coll. Cardiol. 32, 1063–1067.

Durrer, D., Van Dam, R.T., Freud, G.E., Janse, M.J., Meijler, F.L., Arzbaecher, R.C., 1970. Total excitation of the isolated human heart. Circulation 41, 899–912.

Efimov, I.R., Krinsky, V.I., Jalife, J., 1995. Dynamics of rotating vortices in the Beeler-Reuter model of cardiac tissue. Chaos, Solitions Fractals 5, 513–526.

Fenton, F., Karma, A., 1998. Vortex dynamics in three-dimensional continuous myocardium with fiber rotation: filament instability and fibrillation. Chaos 8, 20–47.

Franz, M.R., Swerdlow, C., Liem, L., Schaeffer, J., 1988. Cycle length dependence of human action potential duration in vivo. Effects of single extrastimuli, sudden sustained rate acceleration and deceleration, and different steady-state frequencies. J. Clin. Invest. 82, 972–979.

Garfinkel, A., Qu, Z., 1999. Nonlinear dynamics of excitation and propagation in cardiac tissue. In: Zipes, D.P., Jalife, J. (Eds.), Cardiac Electrophysiology. From Cell to Bedside, third ed. Saunders, Philadelphia, pp. 315–320.

Gettes, L.S., Cascio, W.E., Sanders, W.E., 1995. Mechanisms of sudden cardiac death. In: Zipes, D.P., Jalife, J. (Eds.), Cardiac Electrophysiology. From Cell to Bedside, second ed. Saunders, Philadelphia, pp. 527–538.

Girouard, S.D., Pastore, J.M., Laurita, K.R., Gregory, K.W., Rosenbaum, D.S., 1996. Optical mapping in a new guinea pig model of ventricular tachycardia reveals mechanisms for multiple wavelengths in a single reentrant circuit. Circulation 93, 603–613.

Gray, R.A., Jalife, J., Panfilov, A., Baxter, W.T., Cabo, C., Davidenko, J.M., Pertsov, A.M., 1995. Nonstationary vortexlike reentrant activity as a mechanism of polymorphic ventricular tachycardia in the isolated rabbit heart. Circulation 91, 2454–2469.

Greenstein, J.L., Winslow, R.L., 2002. An integrative model of the cardiac ventricular myocyte incorporating local control of Ca^{2+} release. Biophys. J. 83, 2918–2945.

Hren, R., 1996. A realistic model of the human ventricular myocardium: application to the study of ectopic activation. Ph.D. Thesis, Dalhouse University, Halifax.

Iost, N., Virag, L., Opincariu, M., Szecsi, J., Varro, A., Papp, J.G., 1998. Delayed rectifier potassium current in undiseased human ventricular myocytes. Cardiovasc. Res. 40, 508–515.

Iyer, V., Mazhari, R., Winslow, R., 2004. A computational model of the human left-ventricular epicardial myocyte. Biophys. J. 87, 1507–1525.

Jalife, J., 2000. Ventricular fibrillation: mechanisms of initiation and maintenance. Annu. Rev. Physiol. 62, 25–50.

Jongsma, H.J., Wilders, R., 2000. Gap junctions in cardiovascular disease. Circ. Res. 86, 1193–1197.

Keener, J., Sneyd, J., 1998. Mathematical Physiology. Springer, New York, Heidelberg, Berlin.

Li, G.R., Feng, J., Yue, L., Carrier, M., Nattel, S., 1996. Evidence for two components of delayed rectifier K^+ current in human ventricular myocytes. Circ. Res. 78, 689–696.

Li, G.R., Feng, J., Yue, L., Carrier, M., 1998. Transmural heterogeneity of action potentials and I_{to1} in myocytes isolated from the human right ventricle. Am. J. Physiol. Heart Circ. Physiol. 275, H369–H377.

Li, G., Yang, B., Feng, J., Bosch, R.F., Carrier, M., Nattel, S., 1999. Transmembrane I_{Ca} contributes to rate-dependent changes of action potentials in human ventricular myocytes. Am. J. Physiol. Heart Circ. Physiol. 276, H98–H106.

Luo, C., Rudy, Y., 1991. A model of the ventricular cardiac action potential. Depolarization, repolarization, and their interaction. Circ. Res. 68, 1501–1526.

Luo, C., Rudy, Y., 1994. A dynamic model of the cardiac ventricular action potential. I. Simulations of ionic currents and concentration changes. Circ. Res. 74, 1071–1096.

Morgan, J.M., Cunningham, D., Rowland, E., 1992. Electrical restitution of the endocardium of the intact human right ventricle. Br. Heart. J. 67, 42–46.

Nanthakumar, K., Walcott, G.P., Melnick, S., Rogers, J.M., Kay, M.W., Smith, W.M., Ideker, R.E., Holman, W., 2004. Epicardial organization of human ventricular fibrillation. Heart Rhythm 1, 14–23.

Newton, J., Smith, W., Ideker, R., 2004. Estimated global transmural distribution of activation rate and conduction block during porcine and canine ventricular fibrillation. Circ. Res. 94, 836–842.

Noble, D., Varghese, A., Kohl, P., Noble, P., 1998. Improved guinea-pig ventricular cell model incorporating a diadic space, I_{Kr} and I_{Ks}, and length- and tension-dependent processes. Can. J. Cardiol. 14, 123–134.

Omichi, C., Lamp, S.T., Lin, S., Yang, J., Baher, A., Zhou, S., Attin, M., Lee, M., Karagueuzian, H.S., Kogan, B., Qu, Z., Garfinkel, A., Chen, P., Weiss, J.N., 2004. Intracellular Ca dynamics in ventricular fibrillation. Am. J. Physiol. Heart Circ. Physiol. 286, H1836–H1844.

Panfilov, A.V., Hogeweg, P., 1996. Scroll breakup in a three-dimensional excitable medium. Phys. Rev. E 53, 1740–1743.

Panfilov, A.V., Keener, J.P., 1995. Re-entry in three-dimensional Fitzhugh–Nagumo medium with rotational anisotropy. Physica D 84, 545–552.

Pereon, Y., Demolombe, S., Baro, I., Drouin, E., Charpentier, F., Escande, D., 2000. Differential expression of KvLQT1 isoforms across the human ventricular wall. Am. J. Physiol. Heart Circ. Physiol. 278, H1908–H1915.

Plonsey, R., Barr, R., 1989. Bioelectricity. Plenum Publishing Corporation, New York.

Priebe, L., Beuckelmann, D.J., 1998. Simulation study of cellular electric properties in heart failure. Circ. Res. 82, 1206–1223.

Pruvot, E.J., Katra, R.P., Rosenbaum, D.S., Laurita, K.R., 2004. Role of calcium cycling versus restitution in the mechanism of repolarization alternans. Circ. Res. 94, 1083–1090.

Qu, Z., Garfinkel, A., 1999. An advanced algorithm for solving partial differential equation in cardiac conduction. IEEE Trans. Biomed. Eng. 46, 1166–1168.

Rice, J.J., Jafri, M.S., Winslow, R.L., 1999. Modeling gain and gradedness of Ca^{2+} release in the functional unit of the cardiac diadic space. Biophys. J. 77, 1871–1884.

Rogers, J.M., Huang, J., Melnick, S.B., Ideker, R.E., 2003. Sustained reentry in the left ventricle of fibrillating pig hearts. Circ. Res. 92, 539–545.

Rush, S., Larsen, H., 1978. A practical algorithm for solving dynamic membrane equations. IEEE Trans. Biomed. Eng. 25, 389–392.

Shiferaw, Y., Watanabe, M.A., Garfinkel, A., Weiss, J.N., Karma, A., 2003. Model of intracellular calcium cycling in ventricular myocytes. Biophys. J. 85, 3666–3686.

Shimizu, W., Antzelevitch, C., 1999. Cellular and ionic basis for T-wave alternans under long-QT conditions. Circulation 99, 1499–1507.

Ten Tusscher, K.H.W.J., Panfilov, A.V., 2003. Reentry in heterogeneous cardiac tissue described by the Luo–Rudy ventricular action potential model. Am. J. Physiol. Heart Circ. Physiol. 284, H542–H548.

Ten Tusscher, K.H.W.J., Noble, D., Noble, P.J., Panfilov, A.V., 2004. A model for human ventricular tissue. Am. J. Physiol. Heart Circ. Physiol. 286, H1573–H1589.

Valderrabano, M., Yang, J., Omichi, C., Kil, J., Lamp, S.T., Qu, Z., Lin, S., Karagueuzian, H.S., Garfinkel, A., Chen, P., Weiss, J.N., 2002. Frequency analysis of ventricular fibrillation in swine ventricles. Circ. Res. 90, 213–222.

Volders, P.G.A., Kulcsar, A., Vos, M., Sipido, K., Wellens, H., Lazarra, R., Szabo, B., 1997. Similarities between early and delayed after depolarizations induced by isoproterenol in canine ventricular myocytes. Cardiovasc. Res. 34, 348–359.

Volders, P., Stengl, M., Van Opstal, J.M., Gerlach, U., Spatjens, R., Beekman, J., Sipido, K., Vos, M., 2003. Probing the contribution of iks to canine ventricular repolarization: key role for beta-adrenergic receptor stimulation. Circulation 107, 2753–2760.

Winslow, R.L., Rice, J., Jafri, S., Marban, E., O'Rourke, B., 1999. Mechanisms of Altered Excitation-contraction coupling in canine tachycardia–induced heart failure, II model studies. Circ. Res. 84, 571–586.